

Reconstructing Top Events with p14 Multi-Jet Samples

Michael Begel

University of Rochester, Rochester, NY 14627 USA

(Dated: February 10, 2006)

The cross section for the production of pairs of top quarks was measured in high-multiplicity jet events. The top-quark signal was extracted using the combination of identified b jets and W bosons reconstructed from dijets. The cross section was 12.1 ± 4.9 (stat.) ± 4.6 (sys.) ± 0.8 (lum.) pb assuming $m_t = 175$ GeV. The dependence of the cross section on the top mass was about -0.15 pb/GeV. This cross section is consistent with the Standard Model expectation.

I. INTRODUCTION

The top quark is primarily produced in pairs at the Fermilab Tevatron Collider (Fig. 1). The top quark decays to a W boson and b quark with a branching ratio of $\approx 100\%$ within the Standard Model (Fig. 2). The W boson subsequently decays into a lepton–neutrino or a quark–anti-quark pair. Top events are classified according to the W boson decay channel as shown schematically in Fig. 3. The classic “lepton+jets” channel, for example, has one W boson that decays leptonically to either an e or μ with its associated neutrino while the other W boson decays hadronically to a $u\bar{d}$ or a $c\bar{s}$. Such events are identified in the detector by the presence of a high- p_T lepton, \cancel{E}_T , two b jets, and two light (not- b) jets. The “all-hadronic” or “all-jets” decay channel, with a branching fraction of 0.46, has two b jets and four light jets. The “multi-jet” decay mode, the focus of this analysis, also includes contributions from the τ channels when the τ decays hadronically, as well as the other decay channels when additional jets are produced.

This study is a first attempt to directly reconstruct the top quark decay in its multi-jet mode. There should be enough statistics and a sufficiently well-understood detector in p14 to allow the W -boson and top-quark mass peaks to be reconstructed. These peaks can then be used to extract the production rate of top quarks, measure properties of the $t\bar{t}$ system, search for signatures of new physics with a model-independent methodology, and provide an additional handle on the detector calibration.

Separation of signal from background is critical to achieve these goals. The identification of the b jet from the top decay is used to suppress the multi-jet backgrounds that otherwise swamps $t\bar{t}$ production at the Tevatron. The selection criteria and basic methodology used in this analysis were developed prior to any examination of either data or Monte Carlo

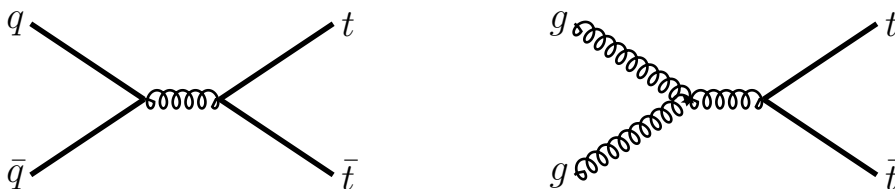


FIG. 1: Dominant production diagrams for $t\bar{t}$ to leading order in α_s at the Fermilab Tevatron Collider. The $q\bar{q}$ annihilation diagram represents $\approx 85\%$ of the total cross section.

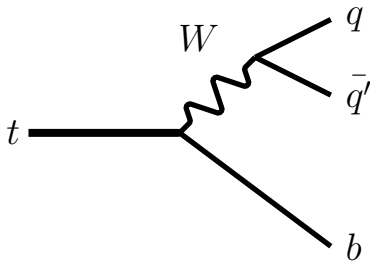


FIG. 2: Sketch of a top decay into a W boson and b quark. The W boson subsequently decays into a quark and an anti-quark.

$\bar{c}s$	lepton + jets	τ + jets	all hadronic		
W^-					
$\bar{u}d$	$\tau e/\tau\mu$	$\tau\tau$	τ + jets		
τ^-					
μ^-	dilepton	$\tau e/\tau\mu$	lepton + jets		
e^-					
	e^+	μ^+	τ^+	$u\bar{d}$	$c\bar{s}$
	W^+				

FIG. 3: Schematic illustrating the different branching fractions for the two W bosons produced in $t\bar{t}$ events. The area of the box is proportional to the branching fraction.

samples. While over a thousand variations were explored in the course of this study, the original sample definition was used for the final result to limit bias. This is referred to within as the “loose 6j base” sample.

II. DATA SAMPLE

The data considered in this analysis were acquired using the multi-jet triggers summarized in Table I. These triggers required several calorimeter towers above 5 GeV at L1, at least three jets above threshold and some H_T at L2, and at least four jets above threshold at L3. Data accumulated with trigger lists 8.10 through 13.21 were considered in this analysis.¹

Events were reconstructed with p14 software versions p14.03.00, p14.03.01, p14.03.02, p14.05.00, p14.05.02, p14.05.02DST, p14.06.00, and p14.06.01 and fixed with p14.fixtmb2.02 (pass 2). Calorimeter-based jets were reconstructed using the Run 2 mid-point cone algorithm with cone radius 0.5 (JCCB) [1]. Events were skimmed by the Common Sample Group using flags set during reconstruction. This analysis is based on the 3JET skim which required one JCCB jet with $p_T^{\text{reco}} > 20$ GeV and two additional JCCB jets with $p_T^{\text{reco}} > 15$ GeV. All three jets were required to be within $|\eta| < 2.6$. The Top Group re-skimmed these data with the additional requirement that the event satisfy at least one of the triggers in Table I

¹ Trigger lists 9.31, 10.00, 10.01, and 10.02 were excluded because of problems with jets in L1 or L2.

TABLE I: Triggers used in this analysis by trigger list version.

Trigger Name	Trigger Lists	Sample ^a Fraction	L1	L2	L3 ^b
4JT10	8.10–8.41	5.7%	CJT(3,5)	3 jets $E_T^{L3} > 8$ GeV	4 jets $E_T^{L3} > 10$ GeV
4JT10	9.20, 9.30, 9.50 10.03–10.36 11.00–11.04	25.7%	CJT(4,5)	3 jets $E_T^{L2} > 8$ GeV $H_T^{L2} > 90$ GeV	4 jets $E_T^{L3} > 10$ GeV
4JT12	12.10–12.37	55.8%	CJT(3,5)	3 jets $E_T^{L2} > 8$ GeV $H_T^{L2} > 50$ GeV	2 jets $E_T^{L3} > 25$ GeV 3 jets $E_T^{L3} > 15$ GeV 4 jets $E_T^{L3} > 12$ GeV
JT2.5JT10L	13.03, 13.10–13.21	12.8%	CJT(3,5)	3 jets $E_T^{L2} > 6$ GeV $H_T^{L2} > 70$ GeV	2 jets $E_T^{L3} > 25$ GeV 3 jets $E_T^{L3} > 15$ GeV 4 jets $E_T^{L3} > 12$ GeV 5 jets $E_T^{L3} > 10$ GeV

^aOnly considering good LBN and runs.

^bJet requirements at L3 overlap so that the 4JT10 and 4JT12 triggers required at least four jets at L3 and the JT2.5JT10L trigger only required five jets.

(amongst others), have a fourth JCCB jet with $p_T^{\text{reco}} > 8$ GeV, and $H_T^{\text{reco}} > 100$ GeV. Thumbnails were processed into the ROOT trees used by the Top Group with the Ipanema_updated version of `top_tree`. The `top_analyze` framework was used to read these trees.

Triggered events were required to be in good luminosity blocks according to the Luminosity system (including trigger quality and reconstruction status) and the JET/MET group. Events were required to be in good runs according to the Calorimeter, SMT, and CFT groups. No requirement was placed on muon run quality. The total integrated luminosity² considered in this analysis was 360 ± 24 pb⁻¹ [2].

Events were required to have a primary vertex, formed from at least 3 tracks, reconstructed within 50 cm of the nominal center of the detector to comply with energy scale constraints. Events that exhibited coherent noise in the calorimeter were removed [?].

JCCB jets were required to have an electromagnetic fraction between 5 and 95%, less than 40% of their energy in the coarse hadronic layers (CHF), hot cell fraction < 10 , and 90% of the total jet energy concentrated into more than one tower. Reconstructed jets required

² The integrated luminosity for good LBN and runs was determined using Online Luminosity-system tools instead of the `top_dq` package.

confirmation by L1: $[\sum E_T^{L1}]/[(1-\text{CHF}) p_T] > 0.4$ for $|\eta^{\text{det}}| < 0.8$ or $|\eta^{\text{det}}| > 1.5$ (> 0.2 for $0.8 < |\eta^{\text{det}}| < 1.5$).³ Jets were required to have at least two tracks, reconstructed within the jet cone, that pointed to the primary vertex (taggable) [3]. Jet energies were corrected by v5.3 of the jet energy scale (JES) calibration [4]. (The muon-in-jet correction was not applied to these jets.)

III. ANALYSIS

A. Candidates

Events were required to have at least six good JCCB jets with at least two jets having $p_T > 45$ GeV, two other jets having $p_T > 20$ GeV, and the rest having $p_T > 15$ GeV. All jets were required to be within $|y| < 2.4$. These requirements were chosen to minimize the impact of the trigger and skim requirements discussed above while still allowing sufficient kinematic phase space to reconstruct the W mass peak. No vetoes were applied for high- p_T leptons or \cancel{E}_T . This is the base event sample.

Candidate $t\bar{t}$ events, defined on the base sample, required at least two jets with $p_T > 45$ GeV tagged as b jets with the SVT [5] algorithm.⁴ The other jets were required to not be identified as b -tagged jets by this definition. This is the “loose” event sample. Additional samples with requirements on topological variables were considered for systematic studies. Two samples in particular, a “medium” and a “tight” sample, were defined as described in Table II. Cuts on aplanarity (\mathcal{A}), centrality (\mathcal{C}), sphericity (\mathcal{S}), and the ΔR between the

TABLE II: Definition of loose, medium, and tight samples for use in this analysis.

Requirement	Loose	Medium	Tight
aplanarity	none	$\mathcal{A} > 0.05$	$\mathcal{A} > 0.05$
centrality	none	$\mathcal{C} > 0.6$	$\mathcal{C} > 0.7$
sphericity	none	$\mathcal{S} > 0.2$	$\mathcal{S} > 0.5$
$\Delta R_{b\bar{b}}$	none	$\Delta R_{b\bar{b}} > 1$	$\Delta R_{b\bar{b}} > 2$

³ Unlike inclusive-jet analyses, jets with $\sum E_T^{L1} > 55$ GeV were not automatically confirmed.

⁴ This is the tight definition used by the Top Group.

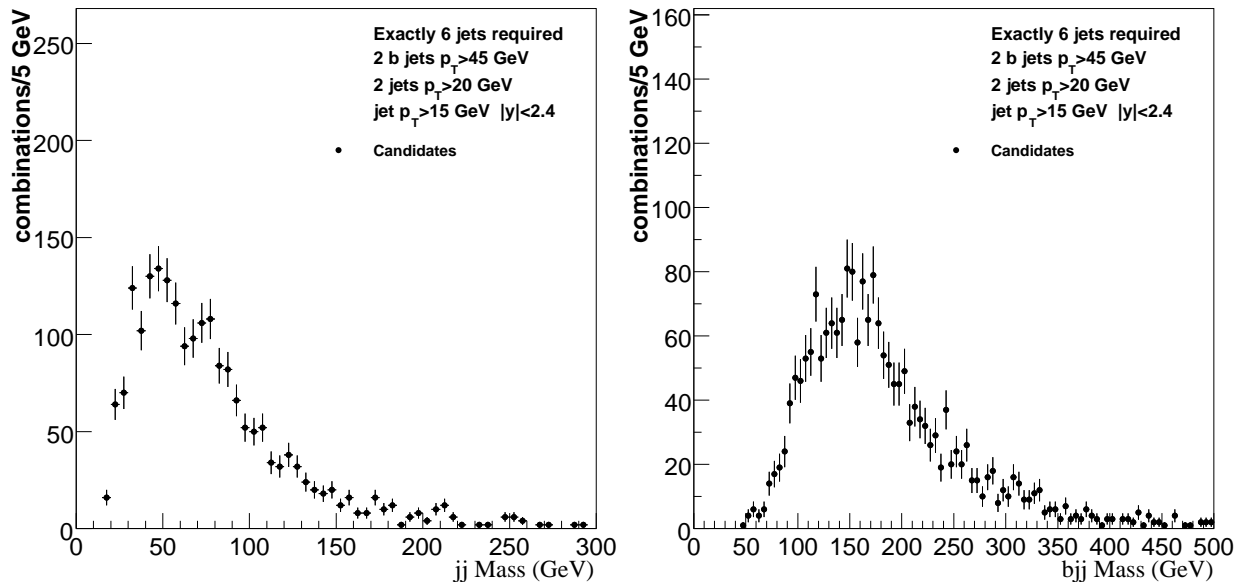


FIG. 4: Mass distributions from the loose $6j$ base data sample. Left: the dijet mass spectrum for all pairs of non- b tagged jets. Right: the three-jet mass spectrum for all combinations of one b -tagged jet and two non- b tagged jets.

two b jets ($\Delta R_{b\bar{b}}$) were used to select top-like events.

This analysis is concentrated on the six-jet multiplicity bin. For the $6j$ sample, exactly two jets were b -tagged and exactly four jets were not. Other multiplicity samples, with similar naming conventions, were considered for systematic studies. For example, the $6 + j$ sample required at least two b -tagged jets and at least four not-tagged jets.

The dijet mass distribution (two non- b tagged jets) and the three-jet mass distribution ($bjj =$ one b -tagged jet and two non- b tagged jets) are shown in Fig. 4. All possible combinations of jets were entered into each mass distribution. Strong fluctuations are visible in the dijet mass distribution near the mass of the W boson and in the bjj mass distribution near the top-quark mass.

B. Background

The dominant backgrounds to $t\bar{t}$ production in the all-hadronic decay channel are multi-jet QCD production and electroweak W boson production with associated jets. Unfortunately, multi-jet QCD generators are not considered reliable for large jet multiplicities and the statistics in the available $b\bar{b}$ and $Wb\bar{b} + \text{jets}$ samples were extremely limited. Background distributions were therefore derived from the data.

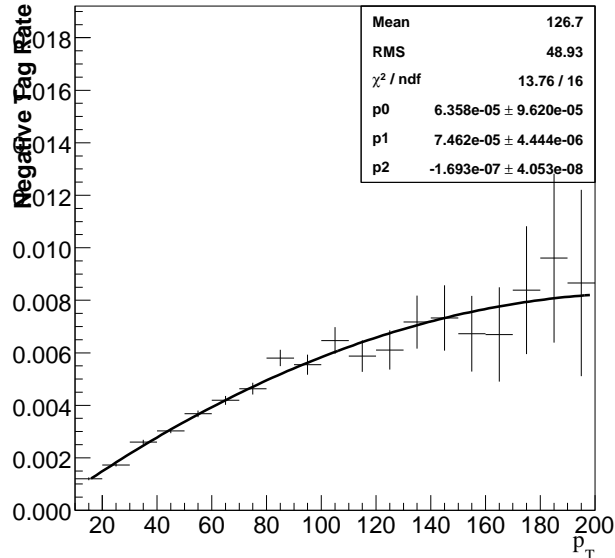


FIG. 5: The negative tag rate function extracted from the $6 + j$ loose data sample. The points are the ratio of the jet p_T spectra for jets that satisfied the negative SVT tag to that for all jets in the sample. The points were fit to a second-order polynomial function.

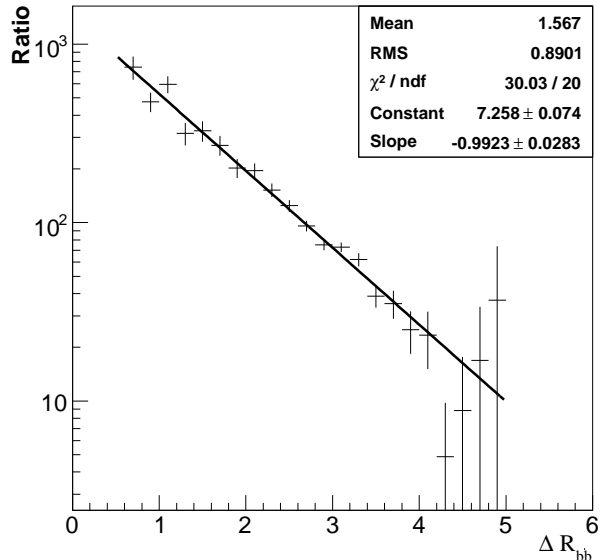


FIG. 6: Weight factor as a function of the distance between two b jets from a $4j$ data sample. The ΔR_{bb} distribution for the candidate sample was divided by the ΔR_{bb} distribution in the background sample (weighted first by the function displayed in Fig. 5). The points were fit to an exponential function.

Two jets in each base sample event were chosen at random and defined to be b jets irrespective of their actual tag status (both jets still had to satisfy the b -jet p_T requirement). Background events were otherwise treated exactly the same as the candidates, including the requirements on the b and non- b jets. Kinematic correlations between b -tagged jets were not completely modeled by the random jet sample, therefore two weights were applied to the jets in the background sample. One was based on the b -jet p_T spectrum, and the other on the angular correlation between the two b -tagged jets (ΔR_{bb}). The p_T -dependent weight was derived from jets that had SVT tags with negative lifetime in the $6 + j$ sample. The ratio of the negative-tag jets to all jets is shown in Fig. 5. This result is similar to the negative tag rate derived as part of the SVT tagger certification [5]. The $4j$ sample, dominated by multi-jet QCD events, was used to extract a weight as a function of ΔR_{bb} . The ratio of the candidate sample to the background sample in $4j$ events is displayed in Fig. 6. The $4j$ background sample was weighted p_T -dependent function shown in Fig. 5. The cross section changed by $< 15\%$ by including these weight factors.

The background sample was normalized to the candidate sample using the jj and bjj mass distributions. Specifically, the background dijet distribution was scaled to the candidate distribution so that the area with $M_{jj} < 65$ GeV was equal. This normalization factor was then adjusted downwards to avoid large negative deviations in the background-subtracted result. The normalization factor was reduced in 1% increments until the sum of the negative bins in the bjj background-subtracted mass distribution was less than half the significance as follows:

$$\frac{1}{2} \sum_{i=1}^{\#bins} \left(|N_{bjj}^{\text{signal}}(i)| - N_{bjj}^{\text{signal}}(i) \right) \leq \frac{1}{2} \frac{N_{bjj}^{\text{signal}}}{\sqrt{N_{bjj}^{\text{candidates}}}}.$$

The jj and bjj mass distributions are shown in Fig. 7 (and Fig. 8) with overlaid, normalized, background samples. The candidate distributions are significantly above background in the W -boson and t -quark mass ranges, respectively.

IV. MONTE CARLO SIMULATION

A. Samples

Two $t\bar{t}$ generators were used in this analysis: ALPGEN v1.3 [6] and PYTHIA v6.2 [7, 8]. The top quark, generated with $m_t = 175$ GeV, was decayed into Wb in both generators. The W bosons in ALPGEN were decayed into quarks; the W bosons in PYTHIA were decayed inclusively into quarks and leptons. ALPGEN events were passed through PYTHIA for initial-state and final-state radiative effects and for hadronization. EVTGEN [9] and TAUOLA [10] were used to decay heavy mesons and τ leptons respectively. Common sample Monte Carlo settings were used during generation (Tune A). Samples were processed through the full p14 simulation chain (d0gstar, d0sim with PYTHIA minimum bias overlay, d0reco, tmbfixer, and d0correct). Jet energies were corrected using JES v5.3 [4]. Jets were over-smearred in energy during `top_tree` production and some jets were removed based on the probability to reconstruct a jet [?]. The Monte Carlo samples used in this analysis are detailed in Table III.

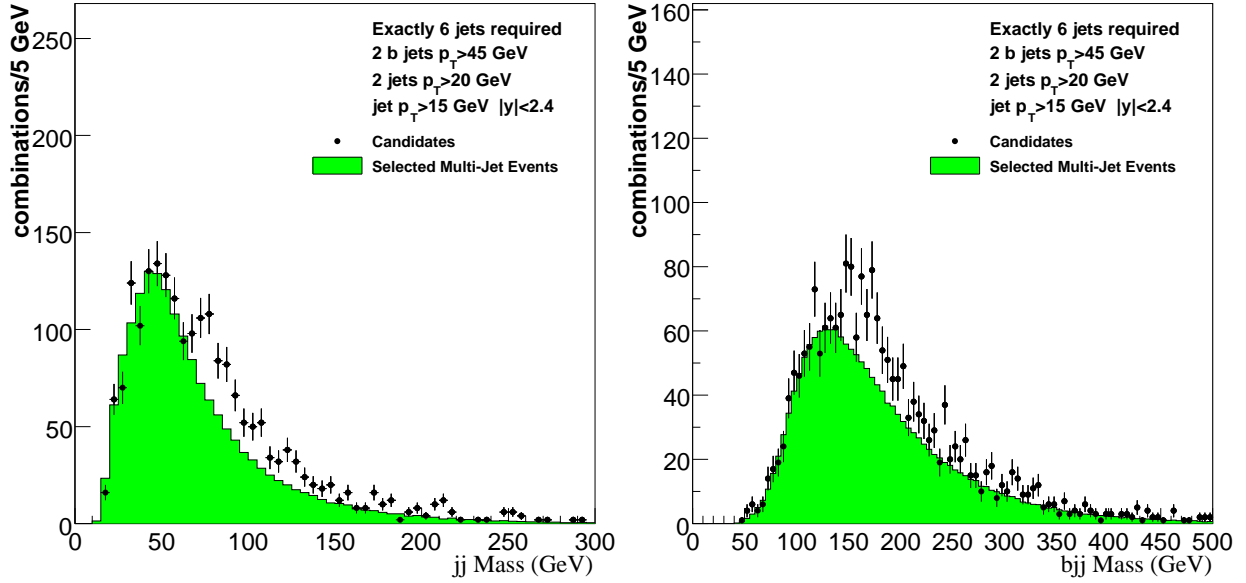


FIG. 7: Mass distributions from the loose $6j$ base data sample. The green-shaded histogram overlaid on the data points is the distribution from the background sample. Left: the dijet mass spectrum for all pairs of non- b tagged jets. Right: the three-jet mass spectrum for all combinations of one b -tagged jet and two non- b tagged jets.

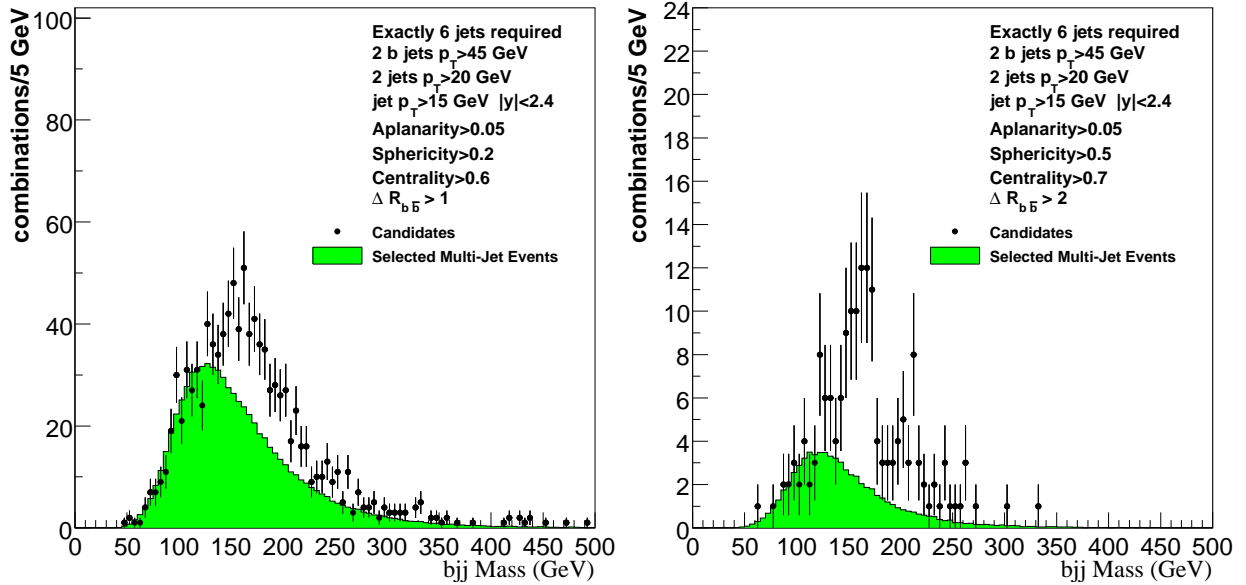


FIG. 8: Three-jet mass distributions from the $6j$ data sample. The green-shaded histogram overlaid on the data points is the distribution from the background sample. Left: the medium sample. Right: the tight sample.

TABLE III: Selection efficiencies for specific Monte Carlo signal samples in the $6j$ multiplicity bin. W bosons were decayed inclusively in PYTHIA; they were decayed into quarks in ALPGEN. (The ratio of candidate events to those in the base sample was 0.3% in the data.)

Generator	Top Mass Cross Section		Events	Event Selection	
	(GeV)	(pb)		base	loose
PYTHIA	175	5.6	199,750	7.1%	1.4%
	175	2.7	189,500	14.4%	2.9%
ALPGEN	165	3.6	48,250	13.0%	2.4%
	185	2.0	56,750	15.3%	3.4%

B. Selection Efficiency

The Monte Carlo $t\bar{t}$ samples were used to estimate the efficiency for events to survive the requirements described in Sections II and III A. The same jet and event requirements used for the data were applied to the Monte Carlo including b ID. The data skim requirements were also applied to the Monte Carlo samples — the JES was adjusted to approximate that of the data for this purpose (jet 4-vectors were scaled by the inverse of the data correction factors).

As the selection criteria were pure multi-jet requirements and there were no vetoes on high- p_T leptons (especially on τ 's) or on \cancel{E}_T , the ALPGEN all-hadronic samples were not sufficient for estimating the true selection efficiency. A non-negligible fraction of ALPGEN lepton + jet events, particularly for $t\bar{t}$ samples with extra jets and samples of τ + jet where the τ decays hadronically, survived the loose criteria. The PYTHIA sample with inclusively decayed W bosons and τ leptons was therefore used for the efficiency estimates. The ALPGEN samples were used for systematic studies of the mass dependence. (No p14 PYTHIA samples exist with $m_t \neq 175$ GeV.)

1. Trigger Corrections

Trigger efficiencies for the triggers defined in Table I were measured in previous top analyses [11, 12]. The turn-on curves for the individual trigger elements were combined⁵ following the prescription in Ref. [13]. Each Monte Carlo event was randomly assigned a

⁵ This was implemented within the `top_trigger` package.

trigger list according to the sample fractions in Table I. Events were then thrown away according to the resulting trigger probability. The impact of the trigger inefficiency was $\approx 3\%$.

As a systematic cross check, data candidate and background events were corrected for the trigger probabilities. Events were weighted by the inverse of the trigger probability and events with probability less than 10% (weights > 10) were removed to avoid large weights. The efficiency for this requirement was calculated by applying the trigger probability cut-off to the Monte Carlo. The $t\bar{t}$ cross section increased by 12% compared to the result obtained by the method described above.

2. *b*-jet tagging efficiency

The *b*-jet tagging efficiencies were measured using the $t\bar{t}$ Monte Carlo samples described in Table III. Unfortunately, it has been demonstrated by the B ID group that the efficiency in the Monte Carlo is significantly greater than the efficiency in the data [3, 5]. The recommended solution is to apply a per-event scale factor, which accounts for these differences, to the efficiency extracted from the Monte Carlo. The jet tagging efficiency consists of two factorized pieces: taggability and tagger. The efficiency of the taggability requirement depends on sample selection; the efficiency of the tagger should be independent of sample.

As indicated in Sec. II, all the jets in this analysis were required to be taggable instead of just the two *b*-tagged jets. This requirement was imposed to reduce the background due to high jet-multiplicity events arising from multiple interactions [11]. The cross section increased by 25% in the loose sample when the requirement of taggability on all six jets was changed to only requiring taggability for the two *b*-tagged jets. However, in the medium and tight samples, where the background from multiple interactions is suppressed by topological requirements, the cross section decreased by 9% and 8%, respectively. These small changes were well within the statistical uncertainties and so there was no need for an additional per-jet scale factor.

Efficiencies were measured for *b*-jets, *c*-jets, and light jets to be identified as *b*-jets and were parameterized as two-dimensional surfaces in the p_T and rapidity of the jet [14]. The efficiency in the data was extracted from a dijet sample enhanced in $b\bar{b}$ content by requiring a soft-muon tagged jet [15], while the Monte Carlo efficiencies were extracted from a $t\bar{t}$

ALPGEN sample in the lepton+jets decay channel. Thus, the probability for a jet with flavor f to be tagged was

$$P(f, p_T, y) = \epsilon_{\text{MC}}^{1+\text{SVT tags}}(f, p_T, y) \frac{\epsilon_{\text{data}}^{1+\text{SVT}\wedge\text{SL tags}}(f, p_T, y)}{\epsilon_{\text{MC}}^{1+\text{SVT}\wedge\text{SL tags}}(f, p_T, y)},$$

where f was determined in the Monte Carlo by identifying a b or c hadron within the jet cone using the event history [14]. The notation “1 + SVT \wedge SL tags” denotes that the efficiency was measured on a sample with at least one soft-lepton tag for a jet of flavor f . Similarly, the notation “1 + SVT tags” denotes that the efficiency was measured without the soft-lepton tag. The negative tagging rate was used to estimate the probability for misidentifying a light flavor (u -, d -, s -quark or gluon) jet as a b -quark jet.

The scale factor for the tagger, S_{SVT} , was defined as

$$S_{\text{SVT}} = \frac{W}{N_{\text{SVT}}^{2+\text{tags}}}$$

where $N_{\text{SVT}}^{2+\text{tags}}$ was the number of Monte Carlo events with two or more SVT tags and

$$W = \sum_{i=1}^{n-1} \sum_{j=i+1}^n P(f_i, p_{T_i}, y_i) P(f_j, p_{T_j}, y_j) \prod_{\substack{k=1 \\ k \neq i \\ k \neq j}}^n \left(1 - P(f_k, p_{T_k}, y_k)\right).$$

Only jets that passed the kinematic selection for b -tagged jets were included in the weight factor calculation. Based on this formulation, the scale factor for the loose and medium samples was $S_{\text{SVT}} = 0.57 \pm 0.09$ (assuming a 15% systematic uncertainty [14]). The scale factor for the tight sample was $S_{\text{SVT}} = 0.63$. As shown in Fig. 9, this difference depended on the b -jet p_T requirement whereas the scale factors in the loose and medium samples were relatively flat. The deviation was most likely due to the $\Delta R_{b\bar{b}}$ requirement in the sample definition. The scale factor for the tight sample without the $\Delta R_{b\bar{b}}$ requirement was $S_{\text{SVT}} = 0.55$ and flat as a function of the b jet p_T requirement. Correlations between the two b -tagged jets are therefore relevant at a level comparable to the systematics associated with S_{SVT} . The S_{SVT} calculation assumed that the efficiency for two or more tags was the square of the efficiency for one or more tags,

$$\epsilon^{2+\text{tags}} = (\epsilon^{1+\text{tags}})^2. \quad (4.1)$$

These efficiencies are plotted for two Monte Carlo samples in Figs. 10 and 11. Using the plateau values from the fits, the assumption in Eq. 4.1 was wrong by 8% for the $t\bar{t}$ sample

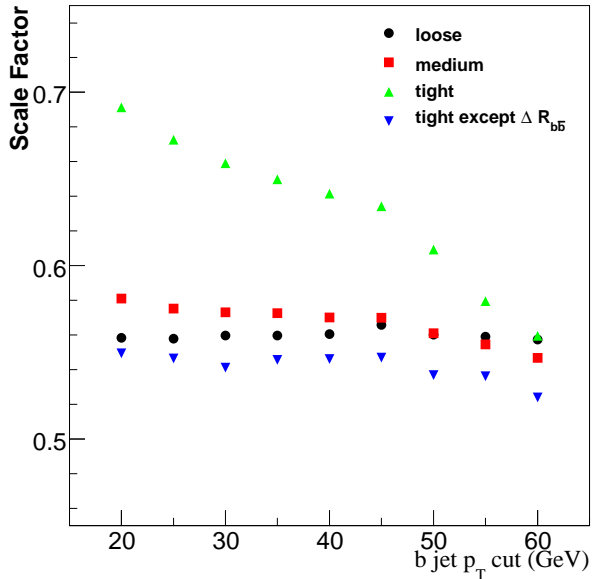


FIG. 9: The scale factor as a function of the b jet p_T requirement for the samples described in Tab. II.

and by $< 1\%$ for the $b\bar{b}$ sample. Including this difference increased the scale factor from 0.57 to $S_{\text{SVT}} = 0.62 \pm 0.11$.

C. Relative Jet Energy Scale

The systematic uncertainty associated with the JES, using the uncertainties for JES v5.3 [4], was approximately a factor of two on the cross section. This is detailed in Table IV where the uncertainties in the data and Monte Carlo were allowed to vary independently. The migration of events across the jet p_T cuts dominated this systematic uncertainty.

The W mass peak in the dijet decay mode (Fig. 7) provides access to the light-jet JES. The position of the W mass peak in the data and Monte Carlo can be used to fix the absolute Monte Carlo JES relative to the data. This is similar to the approach taken in recent top mass analyses [16, 17]. A template fit (TFRACTIONFITTER from ROOT) to the dijet mass distribution displayed in Fig. 7 was performed using the data background (also shown in Fig. 7) and the dijet mass distribution from the PYTHIA $t\bar{t}$ Monte Carlo sample described in Table III. Jet four-vectors in the Monte Carlo were adjusted by a constant

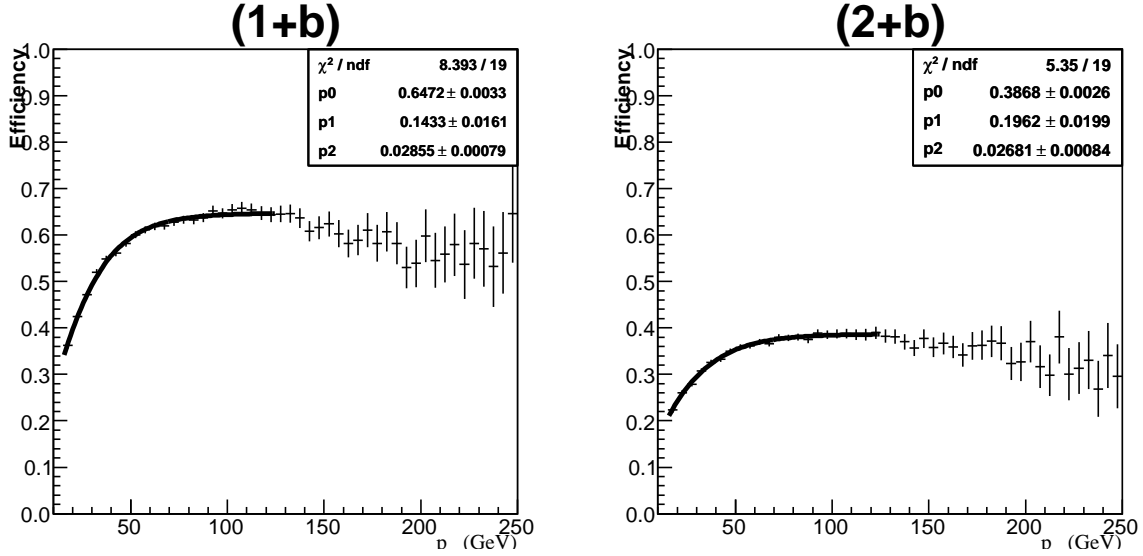


FIG. 10: The efficiency, ϵ_{MC} , when there are one or more identified b jets in the event tagged with SVT (left) or two or more identified b jets (right). The points were extracted from the PYTHIA $t\bar{t}$ Monte Carlo sample. Overlaid on the points are the results to a fit with the functional form $p_0 \tanh(p_1 + p_2 x)$.

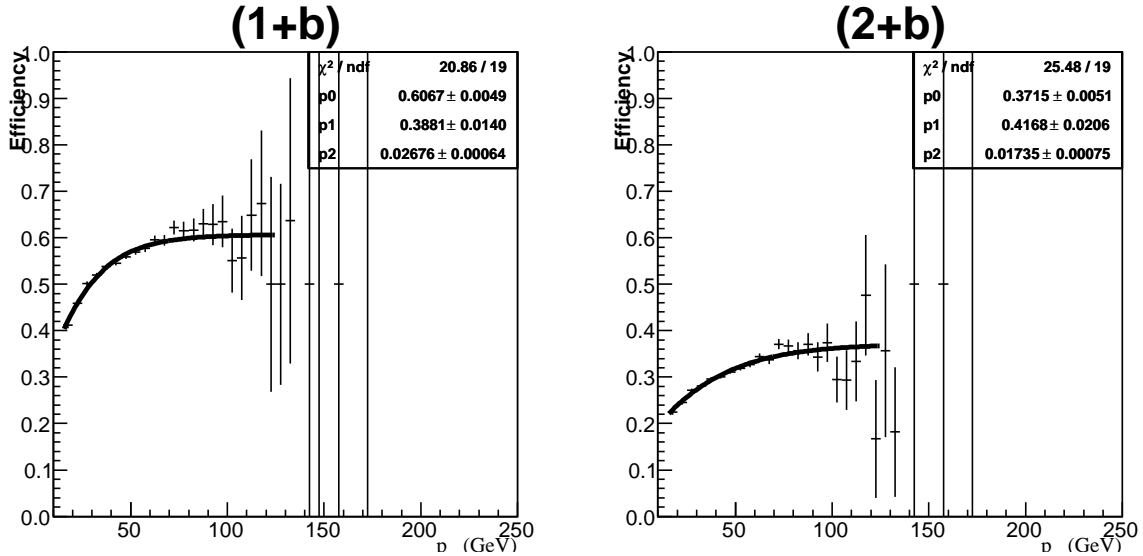


FIG. 11: The efficiency, ϵ_{MC} , when there are one or more identified b jets in the event tagged with SVT (left) or two or more identified b jets (right). The points were extracted from a PYTHIA $b\bar{b}$ Monte Carlo sample requiring $40 < \hat{p}_T < 80$ GeV. Overlaid on the points are the results to a fit with the functional form $p_0 \tanh(p_1 + p_2 x)$.

factor; this JES scale factor was varied from 0.80 to 1.25. The χ^2 of this fit is plotted in Fig. 12 as a function of the JES scale factor. The plot on the left of Fig. 12 is for the standard Monte Carlo sample, the plot on the right is for the Monte Carlo sample with the

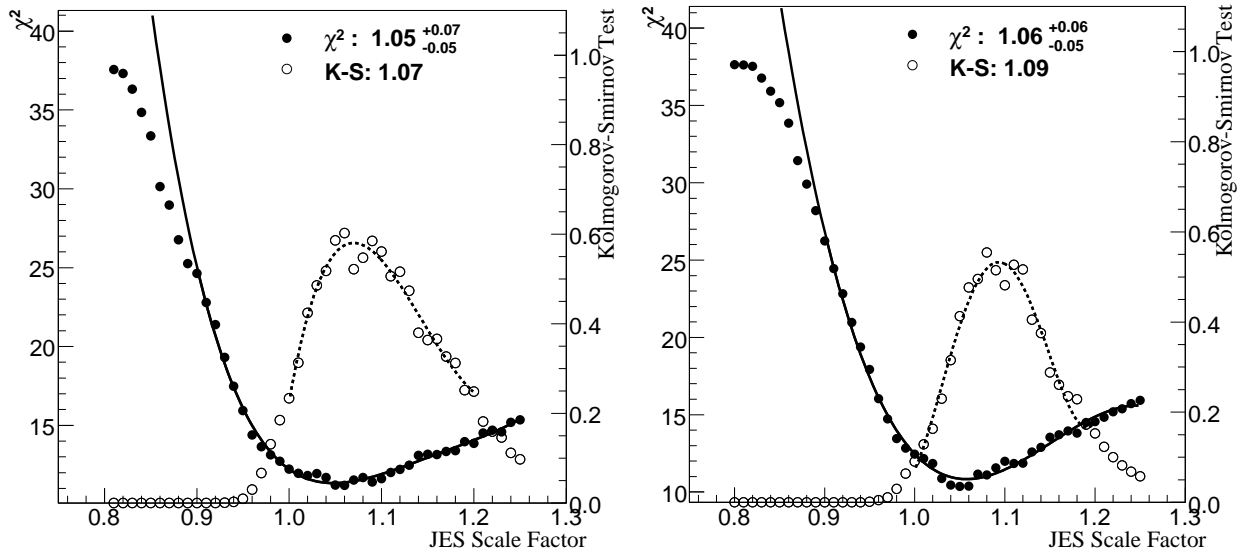


FIG. 12: Result of a template fit to the dijet mass distribution from the $t\bar{t}$ PYTHIA Monte Carlo and the data background distribution to the data candidate distribution. The plot on the right has the Monte Carlo resolution over-smearing disabled; the plot on the left is from the standard sample. The closed circles (\bullet) are the χ^2 of the fit, the open circles (\circ) are the results of the Kolmogorov-Smirnov test.

resolution over-smearing disabled. The minimum χ^2 for the standard sample occurs with a JES scale factor of $1.05^{+0.07}_{-0.05}$. The sample without the resolution over-smearing provides a similar result. Additionally, a Kolmogorov-Smirnov test was applied to the fitted results. This distribution is also plotted in Fig 12 and peaks at 1.07, consistent with the χ^2 result. This results in a systematic uncertainty on the cross section of approximately $\pm 15\%$. The JES scale factors, and the resulting change in the efficiency, are detailed in Table V for the samples described in Table III.

TABLE IV: Change in the cross section relative to the nominal selection as a function of one sigma changes in the data and Monte Carlo jet energy scale corrections. Shifts in the data jet energy corrections were applied to the data; shifts in the Monte Carlo were applied to the Monte Carlo.

		Monte Carlo JES		
		-1	0	+1
Data JES	-1	0.58	0.54	0.49
	0	1.09	1.00	0.91
	+1	1.96	1.80	1.64

TABLE V: Results from template fits to the dijet mass distributions in the Monte Carlo samples described in Table III. The best JES scale factor is listed for each sample and for the sample without resolution over-smearing. The efficiency excludes the scale factor from the previous section.

Generator	Top Mass (GeV)	Resolution Over-smearing?	JES Multiplier	Efficiency (%)	
				default	best
PYTHIA	175	yes	$1.05^{+0.07}_{-0.05}$	1.4	1.5
		no	$1.06^{+0.06}_{-0.05}$	1.4	1.6
ALPGEN	175	yes	$1.08^{+0.06}_{-0.05}$	2.9	3.4
		no	$1.05^{+0.05}_{-0.04}$	3.1	3.4
	165	yes	$1.09^{+0.06}_{-0.05}$	2.4	2.9
		no	$1.07^{+0.05}_{-0.05}$	2.4	2.8
	185	yes	$1.05^{+0.07}_{-0.05}$	3.4	3.7
		no	$1.04^{+0.06}_{-0.05}$	3.6	3.9

D. Background Subtraction and Comparison

The background-subtraction technique described in Sec. IIIB is potentially biased as it could possibly subtract signal contributions at low mass. The fraction of the signal that survived this procedure, the purity (\mathcal{P}), was determined with the $t\bar{t}$ Monte Carlo samples. The data background shapes, normalized to the ratio of the data and Monte Carlo luminosities, were added to the Monte Carlo signal distributions, then subtracted back out through the procedure outlined in Sec. IIIB. The purity was defined as the fraction of events that survived the background subtraction and treated as an efficiency. The purity generally ranged from 75 – 85%. Adjustments by up to 50% in the background normalization changed the cross section by $< 4\%$.

The background-subtracted Monte Carlo mass distributions are compared to the background-subtracted data in Figs. 15 through 18. Additionally, in Figs. 19 through 22, comparisons between the candidates, background, and signal Monte Carlo are presented in aplanarity, sphericity, H_T , centrality, ΔR_{bb} , m_{bb} , p_{Tb} , and p_{Tjj} . The signal samples were normalized to the measured cross sections (Sec. VA).

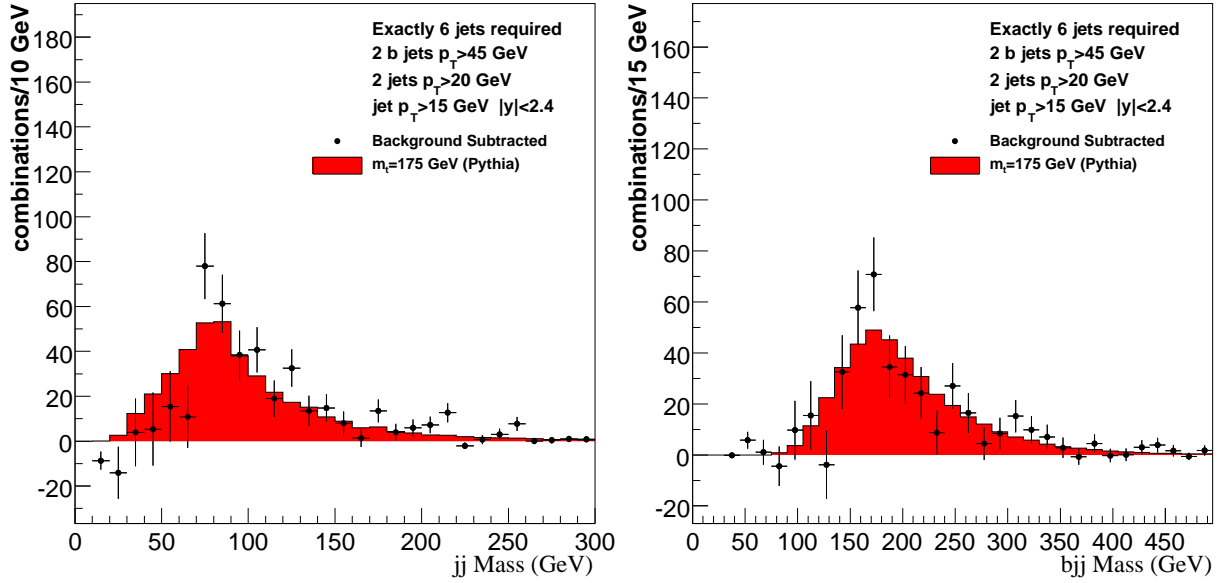


FIG. 13: Mass distributions from the loose $6j$ base sample. The red-shaded histograms overlaid on the background-subtracted data points are the distributions from the PYTHIA signal sample. Left: the dijet mass spectrum for all pairs of non- b tagged jets. Right: the three-jet mass spectrum for all combinations of one b -tagged jet and two non- b tagged jets.

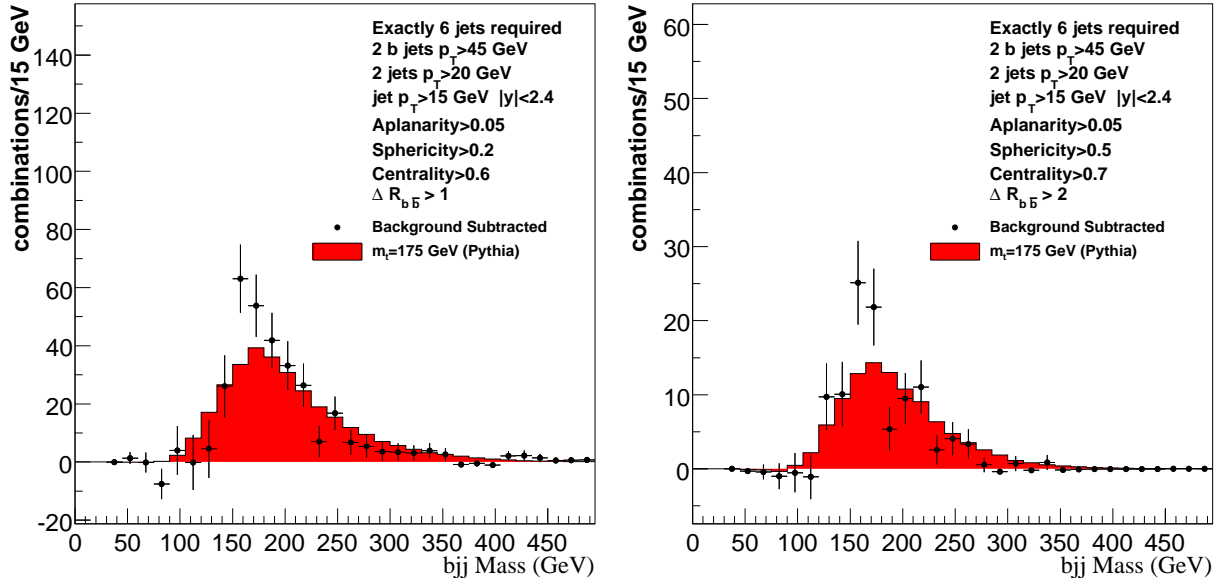


FIG. 14: Three-jet mass distributions from the $6j$ sample. The red-shaded histograms overlaid on the background-subtracted data points are the distributions from the PYTHIA signal sample. Left: the medium sample. Right: the tight sample.

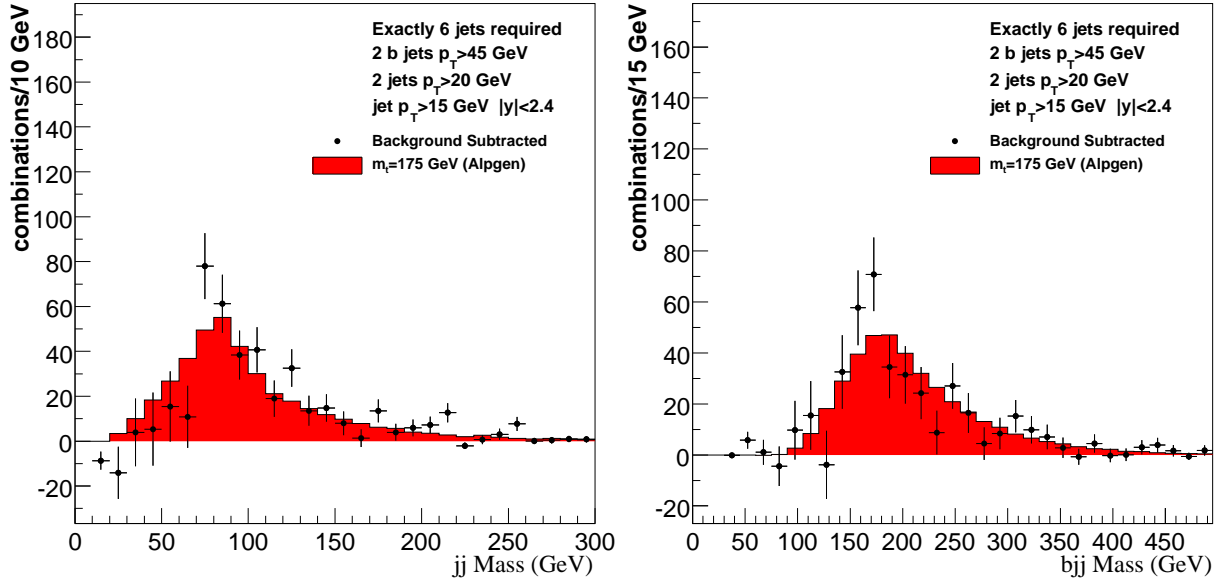


FIG. 15: Mass distributions from the loose $6j$ base sample. The red-shaded histograms overlaid on the background-subtracted data points are the distributions from the ALPGEN signal sample. Left: the dijet mass spectrum for all pairs of non- b tagged jets. Right: the three-jet mass spectrum for all combinations of one b -tagged jet and two non- b tagged jets.

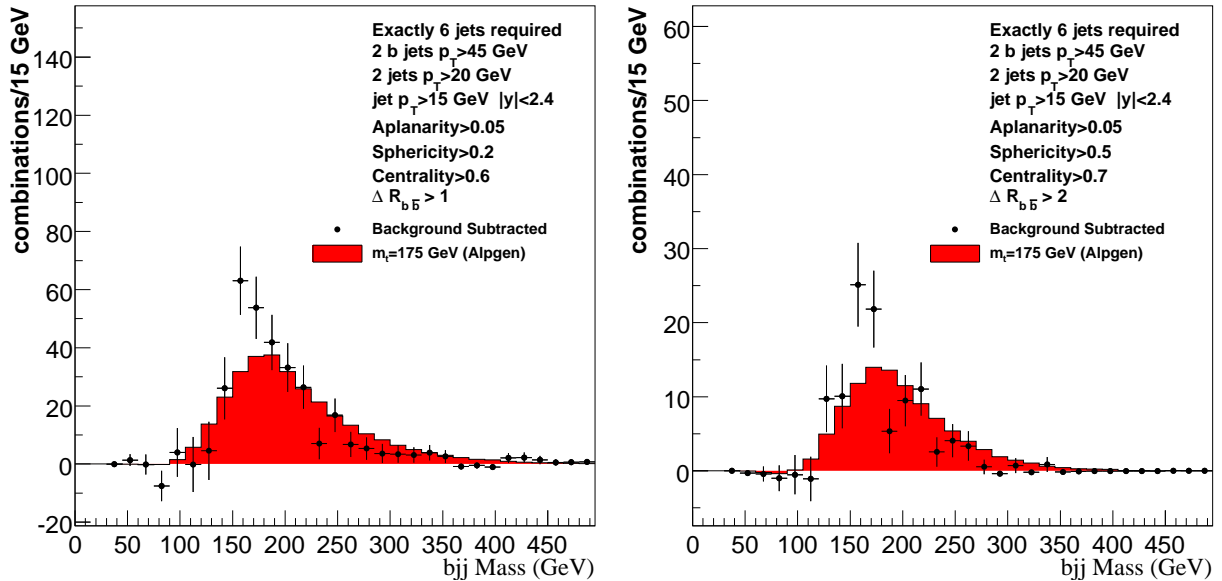


FIG. 16: Three-jet mass distributions from the $6j$ sample. The red-shaded histograms overlaid on the background-subtracted data points are the distributions from the ALPGEN signal sample. Left: the medium sample. Right: the tight sample.

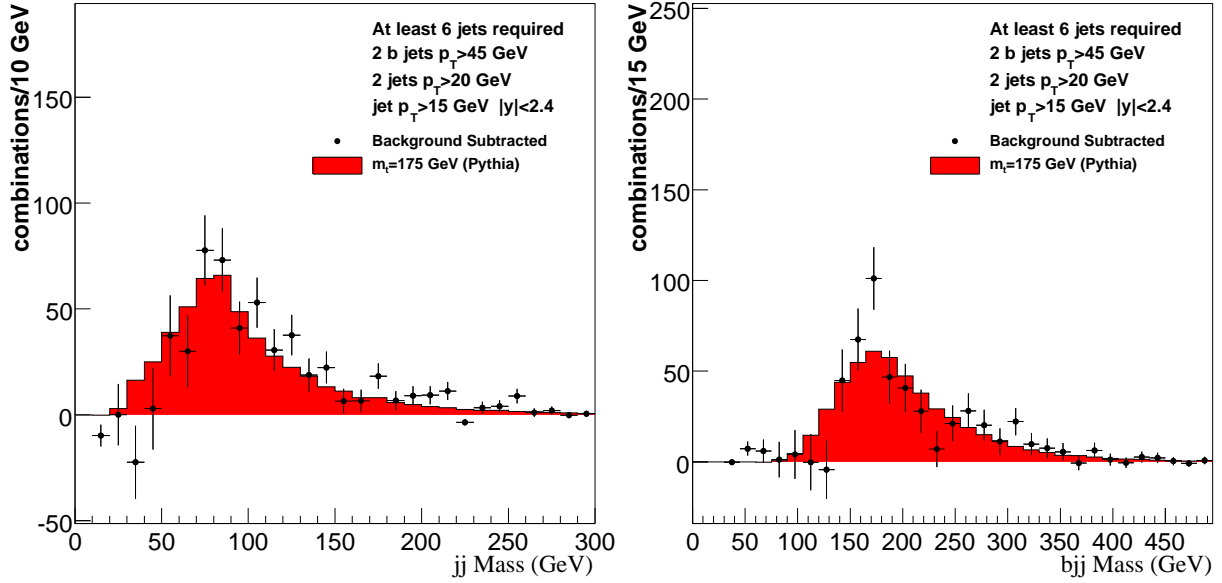


FIG. 17: Mass distributions from the loose $6+j$ base sample. The red-shaded histograms overlaid on the background-subtracted data points are the distributions from the PYTHIA signal sample. Left: the dijet mass spectrum for all pairs of non- b tagged jets. Right: the three-jet mass spectrum for all combinations of one b -tagged jet and two non- b tagged jets.

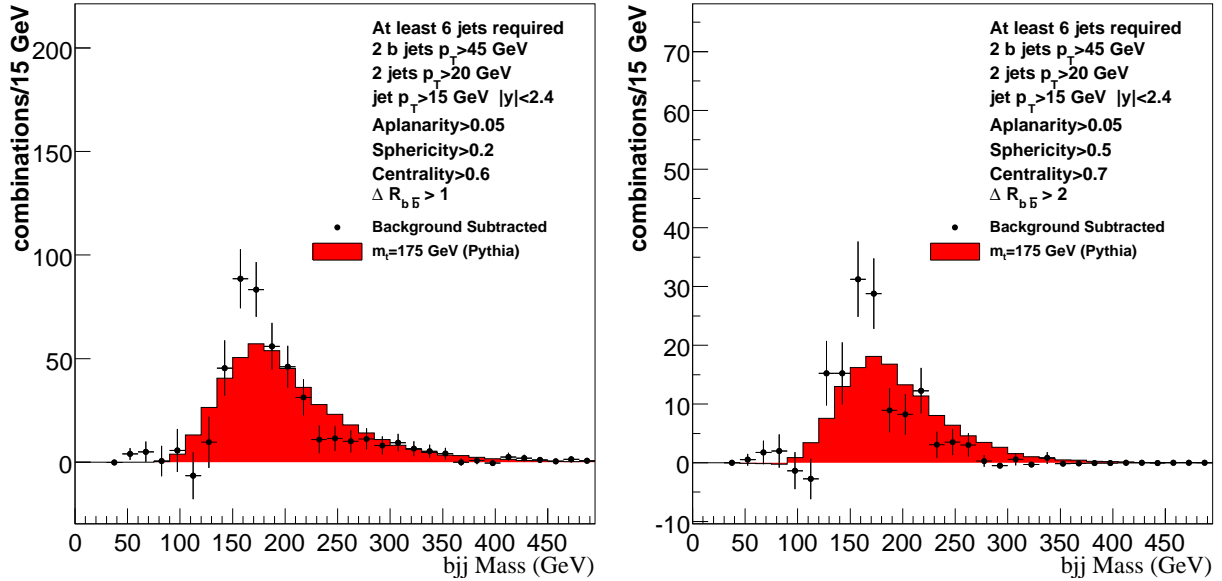


FIG. 18: Three-jet mass distributions from the $6+j$ sample. The red-shaded histograms overlaid on the background-subtracted data points are the distributions from the PYTHIA signal sample. Left: the medium sample. Right: the tight sample.

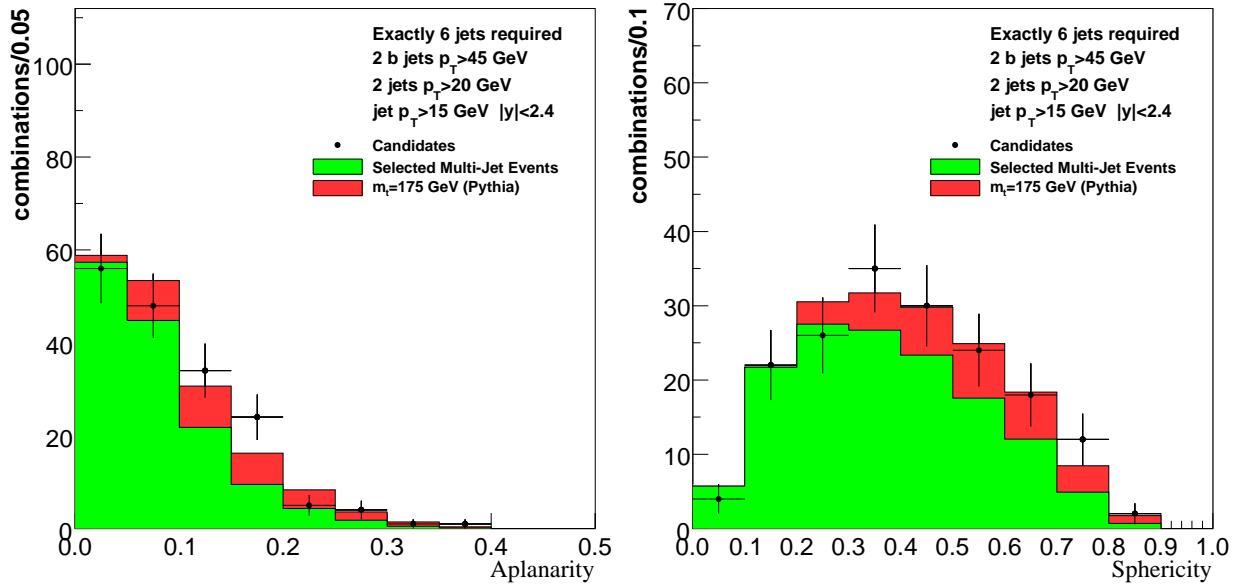


FIG. 19: Distributions from the loose $6j$ base sample. The red-shaded histograms (dark) overlaid on the background-subtracted data points are the distributions from the PYTHIA signal sample. The green-shaded histograms (light) overlaid on the data points are the distributions from the background sample. Left: aplanarity. Right: sphericity.

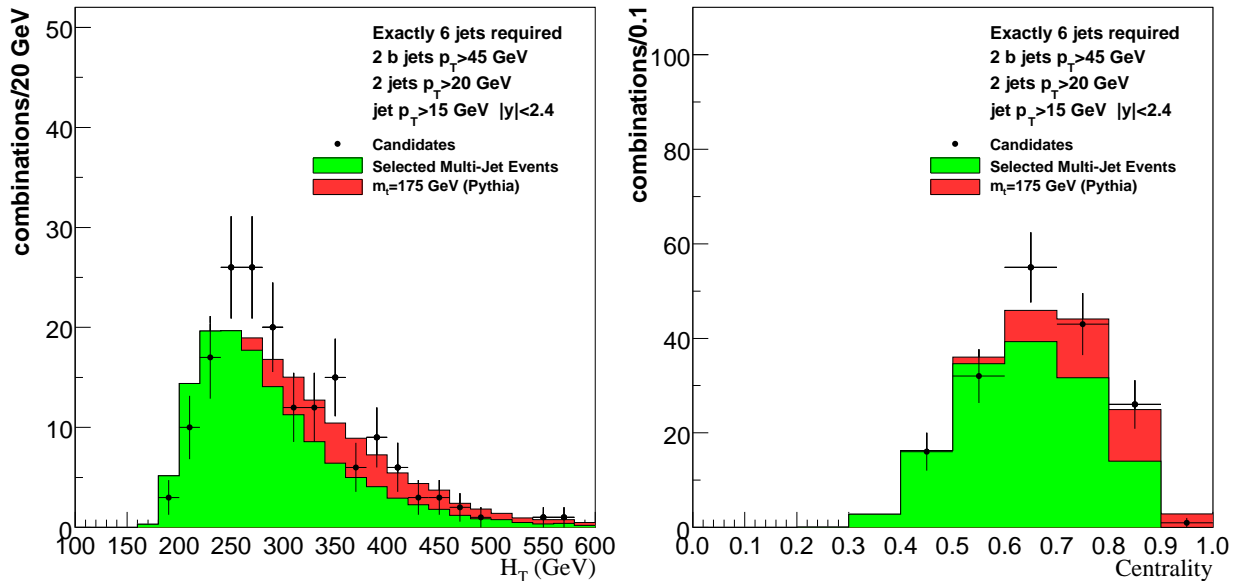


FIG. 20: Distributions from the loose $6j$ base sample. The red-shaded histograms (dark) overlaid on the background-subtracted data points are the distributions from the PYTHIA signal sample. The green-shaded histograms (light) overlaid on the data points are the distributions from the background sample. Left: H_T . Right: centrality.

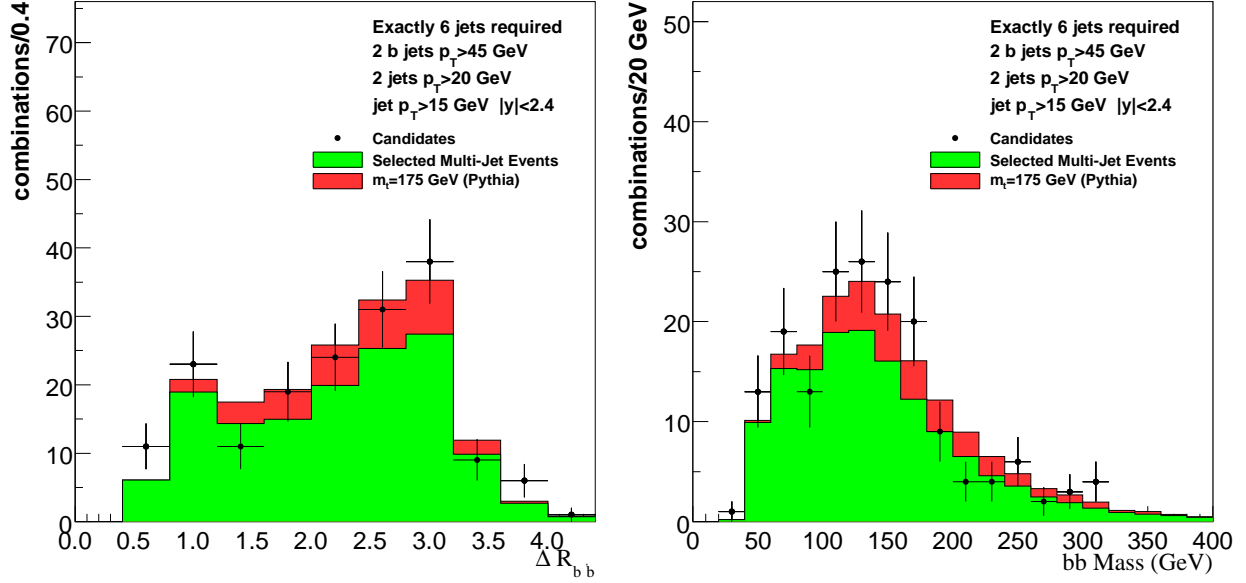


FIG. 21: Distributions from the loose 6j base sample. The red-shaded histograms (dark) overlaid on the background-subtracted data points are the distributions from the PYTHIA signal sample. The green-shaded histograms (light) overlaid on the data points are the distributions from the background sample. Left: ΔR_{bb} . Right: mass of the bb pair.

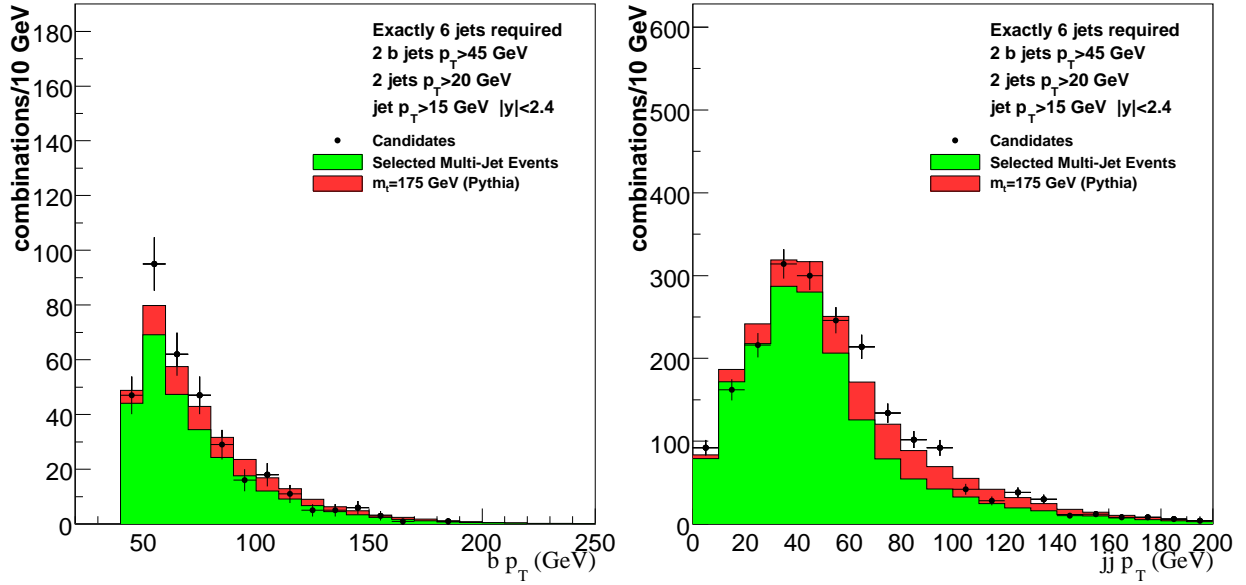


FIG. 22: Distributions from the loose 6j base sample. The red-shaded histograms (dark) overlaid on the background-subtracted data points are the distributions from the PYTHIA signal sample. The green-shaded histograms (light) overlaid on the data points are the distributions from the background sample. Left: b jet p_T . Right: dijet p_T .

V. RESULTS

A. Integrated Cross Section

The cross section for the inclusive production of $t\bar{t}$ was defined as

$$\sigma_{t\bar{t}} = \frac{1}{\mathcal{L}} \frac{(N^{\text{candidates}} - N^{\text{background}})}{\epsilon \mathcal{P} S_{\text{SVT}}}. \quad (5.1)$$

$N^{\text{candidates}}$ was the number of candidates in the sample; $N^{\text{background}}$ was the number of background events normalized by the procedure described in Sec. III B. The luminosity was $\mathcal{L} = 360 \pm 24 \text{ pb}^{-1}$. The selection efficiency, ϵ , was determined from the signal Monte Carlo samples described in Tables III and V. The purity of the signal after background subtraction, \mathcal{P} , was determined by applying the background procedure to the sum of the Monte Carlo signal and the data background as described in Sec. IV D. The efficiency was also adjusted by a scale factor, $S_{\text{SVT}} = 0.62 \pm 0.11$, to account for differences in the b -jet identification between Monte Carlo and data as described in Sec. IV B 2. Values for these quantities, and the computed cross sections, are presented in Tables VI and VII for the $6j$ and $6 + j$ samples, respectively.

The major systematic uncertainties associated with the cross section measurement are shown in Table VIII and were dominated by signal and background modeling and the jet energy scale. The largest systematic uncertainty was due to the background modeling and subtraction ($\pm 25\%$). This uncertainty was estimated primarily by adjusting the criteria used in normalizing the background to the candidate distributions.

The $t\bar{t}$ cross section should not depend on the criteria used to select the sample. In particular, variations in the kinematic and topological criteria should yield equivalent cross sections if the data-based background model and the signal Monte Carlo accurately reflect those variations. In addition to the three topological samples detailed in Table II, thirty-two other sets of topological requirements were also studied. The cross sections measured with these requirements are listed in Tables VI and VII for the $6j$ and $6 + j$ samples, respectively. Additionally, the results from these tables are displayed graphically in Fig. 23. The results in these tables show little evidence of systematic bias associated with these topological requirements. Attempts to reverse the cuts for a few of these requirements (e.g., $\mathcal{A} < 0.05$, $\mathcal{S} < 0.2$) yielded cross sections consistent with zero, as expected.

TABLE VI: Cross section for the inclusive production of pairs of top quarks as a function of topological requirements. These values were measured with the $6j$ sample and used the PYTHIA Monte Carlo ($m_t = 175$ GeV) with a JES scale factor of 1.05 for the efficiency measurement. Only statistical uncertainties are shown.

Sample Definition	$N^{\text{candidates}}$	$N^{\text{background}}$	\mathcal{P} (%)	ϵ (%)	$\sigma_{t\bar{t}}$ (pb)
loose	173 ± 13	140.4 ± 0.8	80	1.51 ± 0.03	12.1 ± 4.9
medium	86 ± 9	60.7 ± 0.5	82	1.17 ± 0.02	11.8 ± 4.3
tight	14 ± 4	5.6 ± 0.1	79	0.37 ± 0.01	12.9 ± 5.8
$H_T > 200$	170 ± 13	138.0 ± 0.8	75	1.51 ± 0.03	12.7 ± 5.2
$\Delta R_{b\bar{b}} > 1$	153 ± 12	122.7 ± 0.7	80	1.45 ± 0.03	11.7 ± 4.8
$S > 0.2$	147 ± 12	116.8 ± 0.8	79	1.46 ± 0.03	11.7 ± 4.7
$S > 0.2 \Delta R_{b\bar{b}} > 1$	131 ± 11	103.3 ± 0.6	79	1.40 ± 0.03	11.1 ± 4.6
$\mathcal{C} > 0.6$	125 ± 11	102.9 ± 0.8	80	1.35 ± 0.03	9.1 ± 4.6
$S > 0.2 \mathcal{C} > 0.6$	118 ± 11	95.5 ± 0.8	80	1.32 ± 0.03	9.5 ± 4.6
$H_T > 200 \mathcal{A} > 0.05$	117 ± 11	89.6 ± 0.7	75	1.33 ± 0.03	12.2 ± 4.8
$\mathcal{A} > 0.05$	117 ± 11	84.5 ± 0.6	79	1.33 ± 0.03	13.8 ± 4.6
$\mathcal{A} > 0.05 S > 0.2$	113 ± 11	81.8 ± 0.6	79	1.32 ± 0.03	13.4 ± 4.6
$\mathcal{C} > 0.6 \Delta R_{b\bar{b}} > 1$	110 ± 10	88.2 ± 0.6	80	1.30 ± 0.03	9.3 ± 4.5
$\Delta R_{b\bar{b}} > 2$	109 ± 10	87.0 ± 0.5	81	1.05 ± 0.02	11.6 ± 5.5
$H_T > 200 \Delta R_{b\bar{b}} > 2$	107 ± 10	85.5 ± 0.5	80	1.05 ± 0.02	11.5 ± 5.5
$S > 0.2 \mathcal{C} > 0.6 \Delta R_{b\bar{b}} > 1$	105 ± 10	81.6 ± 0.6	80	1.27 ± 0.03	10.3 ± 4.5
$\mathcal{A} > 0.05 \Delta R_{b\bar{b}} > 1$	103 ± 10	73.2 ± 0.5	79	1.28 ± 0.03	13.2 ± 4.5
$\mathcal{A} > 0.05 S > 0.2 \Delta R_{b\bar{b}} > 1$	101 ± 10	70.6 ± 0.5	79	1.27 ± 0.03	13.6 ± 4.5
$\mathcal{A} > 0.05 \mathcal{C} > 0.6$	96 ± 10	70.9 ± 0.6	79	1.22 ± 0.02	11.6 ± 4.5
$\mathcal{A} > 0.05 \mathcal{C} > 0.6 \Delta R_{b\bar{b}} > 1$	86 ± 9	60.0 ± 0.5	82	1.18 ± 0.02	12.0 ± 4.3
$H_T > 200 \mathcal{A} > 0.05 \Delta R_{b\bar{b}} > 2$	70 ± 8	53.3 ± 0.4	80	0.90 ± 0.02	10.4 ± 5.2
$\mathcal{A} > 0.05 \Delta R_{b\bar{b}} > 2$	70 ± 8	49.8 ± 0.4	83	0.90 ± 0.02	12.2 ± 5.0
$\mathcal{C} > 0.7$	70 ± 8	46.3 ± 0.5	81	1.02 ± 0.02	12.7 ± 4.5
$\mathcal{A} > 0.05 \mathcal{C} > 0.7$	60 ± 8	42.3 ± 0.5	82	0.93 ± 0.02	10.3 ± 4.5
$S > 0.5$	56 ± 7	32.3 ± 0.4	75	0.75 ± 0.02	18.8 ± 5.9
$\mathcal{A} > 0.05 S > 0.5$	52 ± 7	25.6 ± 0.3	75	0.72 ± 0.02	21.6 ± 5.9
$\mathcal{C} > 0.7 \Delta R_{b\bar{b}} > 2$	41 ± 6	31.0 ± 0.3	83	0.70 ± 0.02	7.7 ± 4.9
$S > 0.5 \mathcal{C} > 0.7$	35 ± 6	18.0 ± 0.3	75	0.61 ± 0.02	16.8 ± 5.9
$\mathcal{A} > 0.05 \mathcal{C} > 0.7 \Delta R_{b\bar{b}} > 2$	33 ± 6	22.7 ± 0.3	85	0.62 ± 0.02	8.7 ± 4.9
$H_T > 200 \mathcal{A} > 0.05 S > 0.5 \mathcal{C} > 0.7$	33 ± 6	15.4 ± 0.3	73	0.59 ± 0.02	18.3 ± 6.0
$\mathcal{A} > 0.05 S > 0.5 \mathcal{C} > 0.7$	33 ± 6	14.5 ± 0.2	76	0.59 ± 0.02	18.4 ± 5.7
$S > 0.5 \Delta R_{b\bar{b}} > 2$	30 ± 5	16.6 ± 0.2	78	0.47 ± 0.02	16.2 ± 6.6
$\mathcal{A} > 0.05 S > 0.5 \Delta R_{b\bar{b}} > 2$	27 ± 5	13.4 ± 0.2	78	0.45 ± 0.02	17.1 ± 6.6
$S > 0.5 \mathcal{C} > 0.7 \Delta R_{b\bar{b}} > 2$	15 ± 4	6.3 ± 0.1	77	0.38 ± 0.01	13.1 ± 5.9
$H_T > 200 \mathcal{A} > 0.05 S > 0.5$	14 ± 4	6.1 ± 0.1	76	0.37 ± 0.01	12.6 ± 6.0
$\mathcal{C} > 0.7 \Delta R_{b\bar{b}} > 2$					

TABLE VII: Cross section for the inclusive production of pairs of top quarks as a function of topological requirements. These values were measured with the $6+j$ sample and used the PYTHIA Monte Carlo ($m_t = 175$ GeV) with a JES scale factor of 1.05 for the efficiency measurement. Only statistical uncertainties are shown.

Sample Definition	$N^{\text{candidates}}$	$N^{\text{background}}$	\mathcal{P} (%)	ϵ (%)	$\sigma_{t\bar{t}}$ (pb)
loose	212 ± 15	181.6 ± 1.0	72	1.92 ± 0.03	9.9 ± 4.7
medium	111 ± 11	82.9 ± 0.7	76	1.50 ± 0.03	11.0 ± 4.1
tight	17 ± 4	7.4 ± 0.1	76	0.47 ± 0.02	12.1 ± 5.2
$H_T > 200$	209 ± 14	180.8 ± 1.0	71	1.92 ± 0.03	9.2 ± 4.7
$\Delta R_{b\bar{b}} > 1$	189 ± 14	159.1 ± 0.8	76	1.85 ± 0.03	9.5 ± 4.4
$\mathcal{S} > 0.2$	180 ± 13	143.8 ± 0.9	72	1.85 ± 0.03	12.2 ± 4.5
$\mathcal{S} > 0.2 \Delta R_{b\bar{b}} > 1$	162 ± 13	129.3 ± 0.7	76	1.78 ± 0.03	10.8 ± 4.2
$\mathcal{C} > 0.6$	153 ± 12	129.6 ± 0.9	76	1.72 ± 0.03	8.0 ± 4.2
$H_T > 200 \mathcal{A} > 0.05$	147 ± 12	113.5 ± 0.8	72	1.71 ± 0.03	12.2 ± 4.4
$\mathcal{A} > 0.05$	147 ± 12	109.1 ± 0.8	72	1.71 ± 0.03	13.7 ± 4.4
$\mathcal{S} > 0.2 \mathcal{C} > 0.6$	146 ± 12	118.9 ± 0.9	76	1.68 ± 0.03	9.4 ± 4.2
$\mathcal{A} > 0.05 \mathcal{S} > 0.2$	143 ± 12	105.9 ± 0.8	72	1.69 ± 0.03	13.6 ± 4.4
$\mathcal{C} > 0.6 \Delta R_{b\bar{b}} > 1$	136 ± 12	111.6 ± 0.8	76	1.65 ± 0.03	8.6 ± 4.1
$\mathcal{S} > 0.2 \mathcal{C} > 0.6 \Delta R_{b\bar{b}} > 1$	131 ± 11	105.1 ± 0.7	76	1.62 ± 0.03	9.4 ± 4.2
$\mathcal{A} > 0.05 \Delta R_{b\bar{b}} > 1$	131 ± 11	96.8 ± 0.6	75	1.65 ± 0.03	12.3 ± 4.1
$\Delta R_{b\bar{b}} > 2$	130 ± 11	109.7 ± 0.5	77	1.32 ± 0.03	8.9 ± 5.0
$\mathcal{A} > 0.05 \mathcal{S} > 0.2 \Delta R_{b\bar{b}} > 1$	129 ± 11	94.8 ± 0.6	75	1.63 ± 0.03	12.5 ± 4.1
$H_T > 200 \Delta R_{b\bar{b}} > 2$	128 ± 11	108.0 ± 0.5	77	1.32 ± 0.03	8.8 ± 5.0
$\mathcal{A} > 0.05 \mathcal{C} > 0.6$	123 ± 11	93.7 ± 0.8	76	1.57 ± 0.03	11.0 ± 4.2
$\mathcal{A} > 0.05 \mathcal{C} > 0.6 \Delta R_{b\bar{b}} > 1$	111 ± 11	82.8 ± 0.7	76	1.51 ± 0.03	11.0 ± 4.1
$H_T > 200 \mathcal{A} > 0.05 \Delta R_{b\bar{b}} > 2$	87 ± 9	66.6 ± 0.5	76	1.15 ± 0.02	10.4 ± 4.8
$\mathcal{A} > 0.05 \Delta R_{b\bar{b}} > 2$	87 ± 9	64.6 ± 0.4	79	1.15 ± 0.02	11.0 ± 4.6
$\mathcal{C} > 0.7$	86 ± 9	65.4 ± 0.7	76	1.28 ± 0.03	9.5 ± 4.3
$\mathcal{A} > 0.05 \mathcal{C} > 0.7$	75 ± 9	55.3 ± 0.6	76	1.17 ± 0.02	9.9 ± 4.3
$\mathcal{S} > 0.5$	67 ± 8	38.5 ± 0.4	69	0.98 ± 0.02	18.8 ± 5.4
$\mathcal{A} > 0.05 \mathcal{S} > 0.5$	63 ± 8	32.2 ± 0.4	70	0.95 ± 0.02	20.9 ± 5.4
$\mathcal{C} > 0.7 \Delta R_{b\bar{b}} > 2$	52 ± 7	42.2 ± 0.4	83	0.86 ± 0.02	6.1 ± 4.5
$\mathcal{A} > 0.05 \mathcal{C} > 0.7 \Delta R_{b\bar{b}} > 2$	43 ± 7	31.2 ± 0.3	82	0.78 ± 0.02	8.3 ± 4.6
$\mathcal{S} > 0.5 \mathcal{C} > 0.7$	40 ± 6	19.8 ± 0.3	71	0.77 ± 0.02	16.4 ± 5.2
$H_T > 200 \mathcal{A} > 0.05 \mathcal{S} > 0.5 \mathcal{C} > 0.7$	38 ± 6	17.3 ± 0.3	68	0.75 ± 0.02	18.0 ± 5.4
$\mathcal{A} > 0.05 \mathcal{S} > 0.5 \mathcal{C} > 0.7$	38 ± 6	16.6 ± 0.3	72	0.75 ± 0.02	17.8 ± 5.1
$\mathcal{S} > 0.5 \Delta R_{b\bar{b}} > 2$	36 ± 6	20.5 ± 0.2	72	0.62 ± 0.02	15.6 ± 6.0
$\mathcal{A} > 0.05 \mathcal{S} > 0.5 \Delta R_{b\bar{b}} > 2$	33 ± 6	17.7 ± 0.2	74	0.59 ± 0.02	15.5 ± 5.8
$\mathcal{S} > 0.5 \mathcal{C} > 0.7 \Delta R_{b\bar{b}} > 2$	18 ± 4	7.9 ± 0.1	74	0.48 ± 0.02	12.5 ± 5.3
$H_T > 200 \mathcal{A} > 0.05 \mathcal{S} > 0.5$	17 ± 4	7.7 ± 0.1	73	0.47 ± 0.02	12.1 ± 5.4
$\mathcal{C} > 0.7 \Delta R_{b\bar{b}} > 2$					

TABLE VIII: Contributions to the systematic uncertainty associated with the $t\bar{t}$ cross section measurement.

Source	Uncertainty (%)
background model & subtraction	± 25
b ID scale factor	± 18
jet energy scale	± 15
Monte Carlo simulation	± 10
trigger	$+12$ -3
purity	± 4
total	± 38

The kinematic requirements were also varied. The b -jet p_T requirement was systematically changed from 35 GeV to 55 GeV. Samples with the leading jet p_T reduced from 45 GeV to 40 GeV, and with the 20 GeV cut reduced to 15 GeV were also studied. Finally, samples where the minimum jet p_T requirement was raised from 15 GeV to 30 GeV were considered. Results from each of these samples, for all 35 topological requirements listed in Table VI, in both the $6j$ and $6 + j$ multiplicity samples, are displayed graphically in Fig. 23. These thousand-plus independent, but correlated, samples yield consistent measurements of the top cross section. This gives additional confidence in the background model and in the Monte Carlo simulation.

The uncertainty on the efficiency was estimated by comparing the difference between the cross sections measured in the $6j$ and $6 + j$ samples (related to the handling of radiative effects) and by comparing the results from PYTHIA and ALPGEN detailed in Table IX.

The cross section for the loose $6j$ base sample (the set of selection criteria chosen prior to beginning this analysis) was 12.1 ± 4.9 (stat.) ± 4.6 (sys.) ± 0.8 (lum.) pb assuming $m_t = 175$ GeV. The dependence of the cross section on the top mass (Table IX) was about -0.15 pb/GeV.

B. $t\bar{t}$ QCD Distributions

The background-subtracted results are compared with QCD expectations in Figs. 24 through 28. For each figure, the same data are overlaid with the results from PYTHIA on the left and ALPGEN on the right. No attempt has been made to unfold the distributions or to compare with NLO calculations. Such comparisons are planned for the p17 analysis.

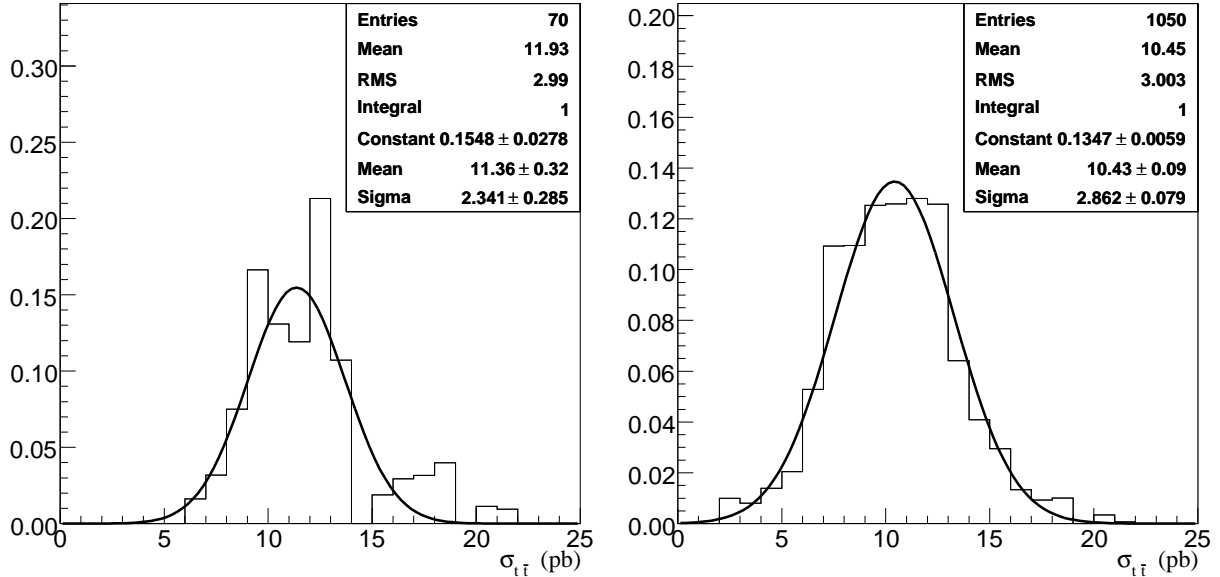


FIG. 23: Distribution of the $t\bar{t}$ cross sections measured with various multiplicity, kinematic, and topological requirements. The figure on the left corresponds to the 70 measurements from Tables VI and VII. The figure on the right represents the cross section for the 35 topological requirements (e.g., Table VI) in the $6j$ and $6 + j$ multiplicity samples with varied kinematic requirements (b -jet p_T ranging from 35 to 55 GeV, 45 GeV light-jet p_T requirement reduced to 40 GeV, 20 GeV light-jet p_T requirement lowered to 15 GeV, light jet p_T requirement ranging from 15 to 30 GeV). All $t\bar{t}$ cross sections were measured independently; the samples are, of course, highly correlated.

TABLE IX: Cross section for the inclusive production of pairs of top quarks as a function of multiplicity, Monte Carlo sample, top mass, and selection criteria. Only statistical uncertainties are shown.

Generator	m_t (GeV)	JES scale factor	$\sigma_{t\bar{t}}$ (pb)					
			$6j$			$6 + j$		
			loose	medium	tight	loose	medium	tight
PYTHIA	175	1.05	12.1 ± 4.9	11.8 ± 4.3	12.9 ± 5.8	9.9 ± 4.7	11.0 ± 4.1	12.1 ± 5.2
	175	1.08	11.0 ± 4.4	10.9 ± 4.0	11.8 ± 5.3	8.7 ± 4.2	10.1 ± 3.8	11.2 ± 4.8
ALPGEN	165	1.09	14.0 ± 5.6	13.4 ± 4.9	15.4 ± 6.9	11.0 ± 5.3	12.7 ± 4.8	14.4 ± 6.2
	185	1.05	10.5 ± 4.2	10.6 ± 3.9	11.4 ± 5.1	8.5 ± 4.1	9.9 ± 3.7	10.8 ± 4.6

VI. CONCLUSIONS

The cross section for the production of pairs of top quarks was measured in high-multiplicity jet events. The top-quark signal was extracted using the combination of SVT-tagged b jets and W bosons reconstructed as dijets. The cross section was $12.1 \pm$

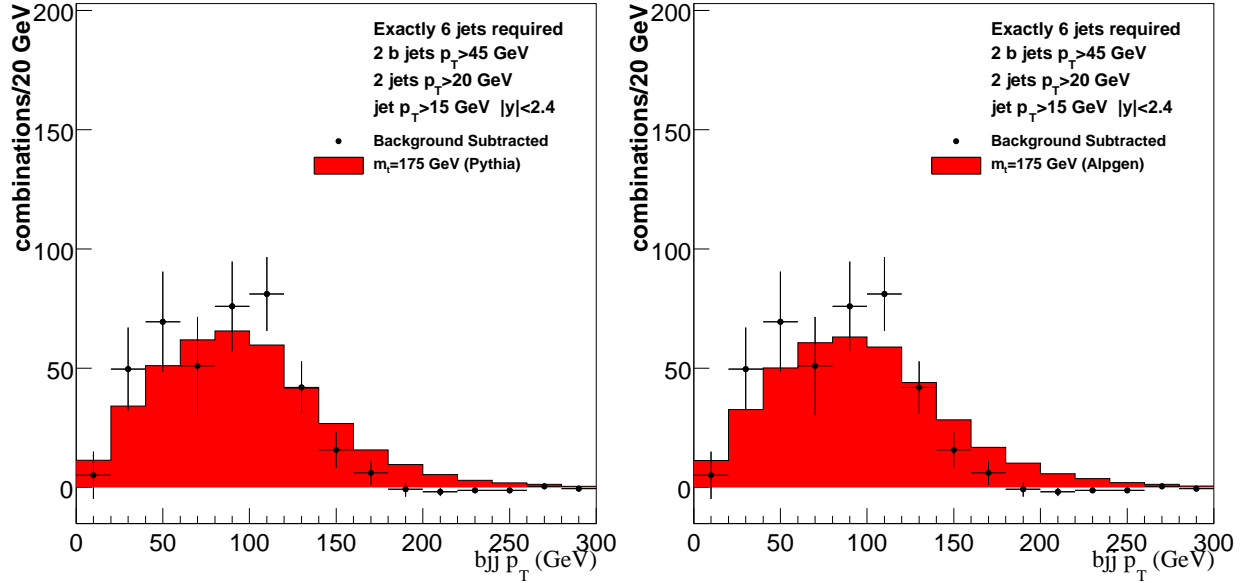


FIG. 24: Top quark p_T distribution. Points are the background-subtracted data from the loose $6j$ base sample. Left: comparison with PYTHIA. Right: comparison with ALPGEN.

$4.9(\text{stat.}) \pm 4.6(\text{sys.}) \pm 0.8(\text{lum.})$ pb assuming $m_t = 175$ GeV. The inclusive production of $t\bar{t}$ has been calculated to NLO in α_s with additional NNLO soft-gluon corrections as $6.77 \pm 0.42(\text{kin.}) \pm 0.20(\text{scale}) \pm 0.45(\text{PDF})$ pb at $m_t = 175$ GeV [18, 19]. The measured integrated cross section is consistent with this Standard Model expectation. Background-subtracted distributions binned in the t -quark p_T , the $t\bar{t}$ mass, p_T , and y , and the $\Delta\phi$ between the top quarks compared reasonably with results from the PYTHIA and ALPGEN Monte Carlo simulations.

-
- [1] G. C. Blazey et al., hep-ex/0005012.
 - [2] T. Edwards et al. (DØ Collaboration), FERMILAB-TM-2278-E.
 - [3] C. Gerber, E. Shabalina, G. Otero y Garzon, “Taggability in p14 pass2 data,” DØ Note 4995.
 - [4] J.-L. Agram et al., “Jet Energy Scale at DØ Run II,” DØ Note 4720.
 - [5] D. Boline, L. Feligioni, and M. Narain, “Update on b -quark jet identification with secondary vertex reconstruction using DØreco version p14 pass2 samples,” DØ Note 4796.
 - [6] M. Mangano et al., JHEP **07**, 001 (2003).
 - [7] T. Sjöstrand et al., Comput. Phys. Commun. **135**, 238 (2001).

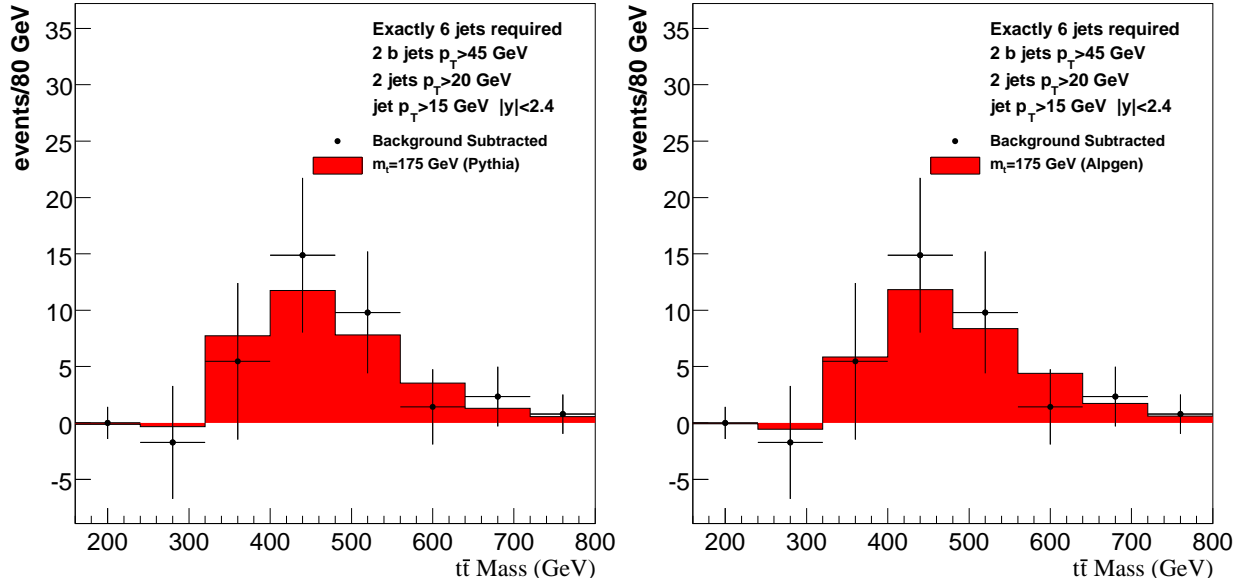


FIG. 25: Mass of the $t\bar{t}$ system. Points are the background-subtracted data from the loose $6j$ base sample. Left: comparison with PYTHIA. Right: comparison with ALPGEN.

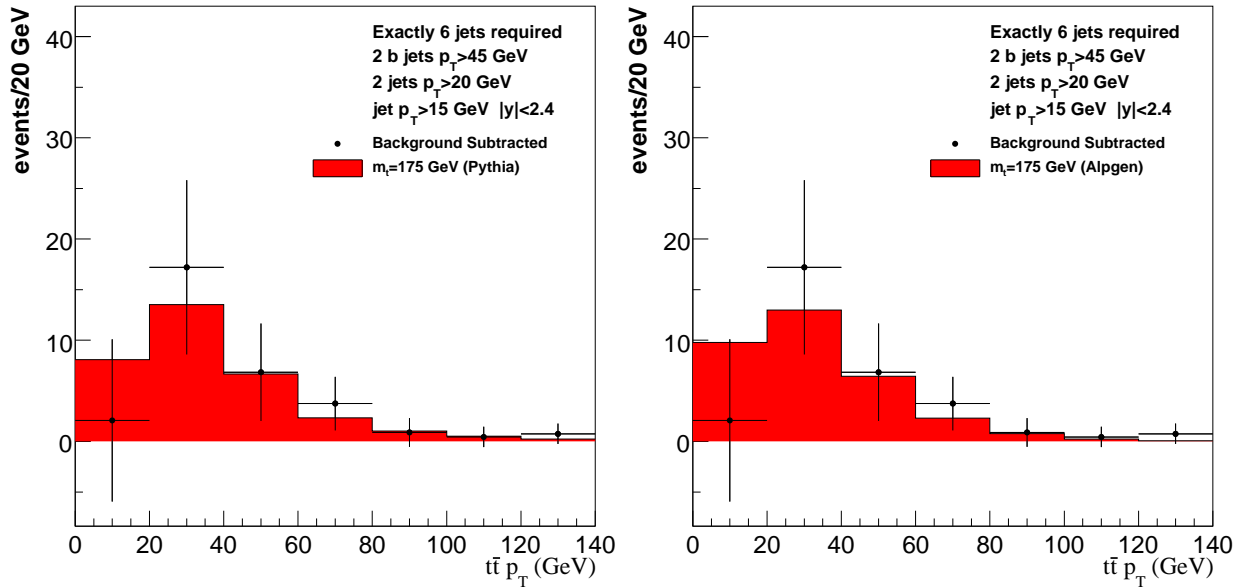


FIG. 26: p_T of the $t\bar{t}$ system. Points are the background-subtracted data from the loose $6j$ base sample. Left: comparison with PYTHIA. Right: comparison with ALPGEN.

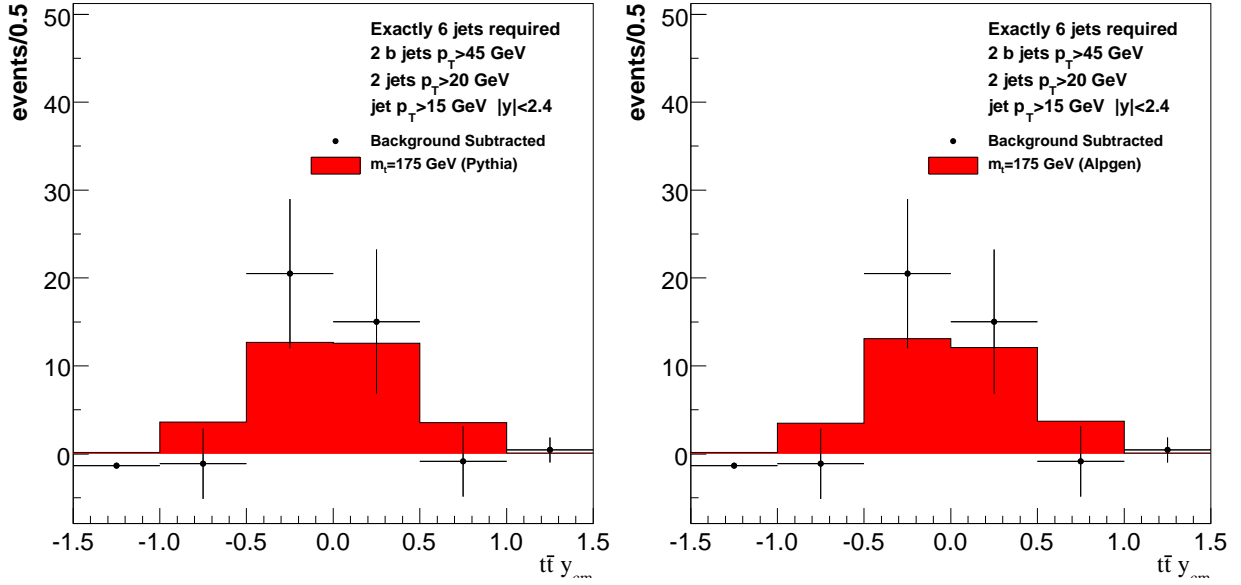


FIG. 27: Rapidity of the $t\bar{t}$ system. Points are the background-subtracted data from the loose $6j$ base sample. Left: comparison with PYTHIA. Right: comparison with ALPGEN.

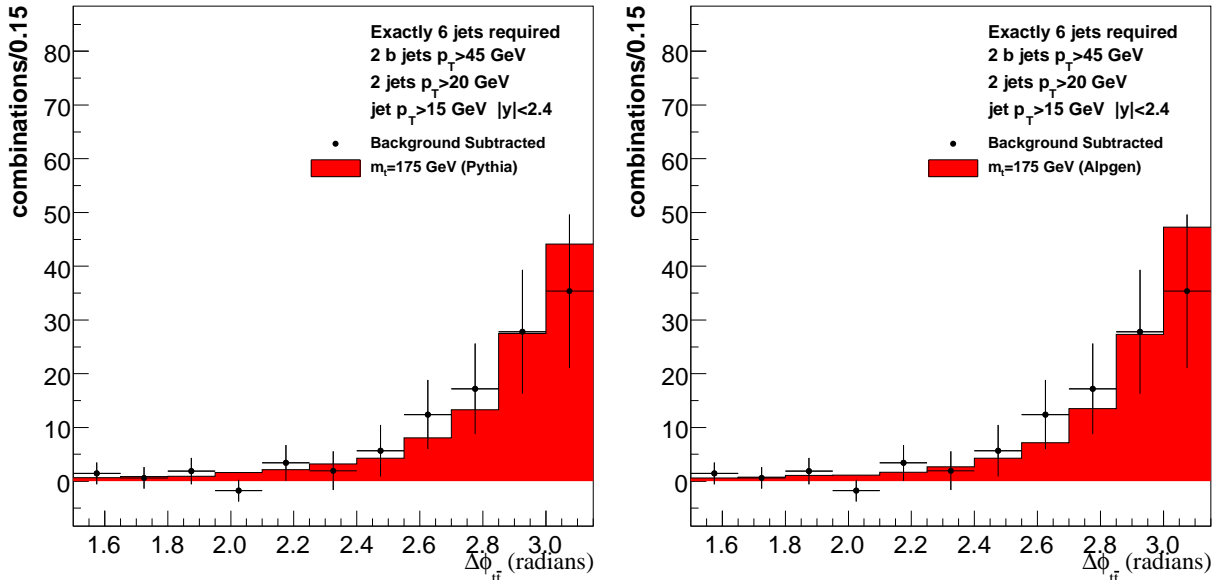


FIG. 28: $\Delta\phi$ between the top quarks. Points are the background-subtracted data from the loose $6j$ base sample. Left: comparison with PYTHIA. Right: comparison with ALPGEN.

- [8] T. Sjostrand, L. Lonnblad, and S. Mrenna (2001), hep-ph/0108264.
- [9] D. J. Lange, Nucl. Instrum. Meth. **A462**, 152 (2001).
- [10] P. Golonka et al. (2003), hep-ph/0312240.
- [11] F. Blekman, “A $t\bar{t}$ cross section measurement in the all-jets channel,” DØ Note 4830.
- [12] F. Blekman, “Turnon curves for the various $t\bar{t}$ to all-jets triggers as measured in multi-jet events in the pass2 dataset,” DØ Note 4847.
- [13] M. Begel et al., “Probability Calculation for Multi-object Trigger Configurations,” DØ Note 4882.
- [14] C. Clement et al., “Measurement of the $t\bar{t}$ production cross section at $\sqrt{s} = 1.96$ TeV using lifetime tagging,” DØ Note 4900.
- [15] K. Hanagaki and J. Kasper, “Identification of b -jet by Soft Muon,” DØ Note 4867.
- [16] M. Mulders and M. Weber, “Top Mass Measurement with b -tagging and Jet Energy Scale Fit in the Lepton+Jets Channel using the Ideogram Method,” DØ Note 4802.
- [17] F. Fielder, A. Magerkurth, and P. Schieferdecker, “Top Quark Measurement with the Matrix Element Method in the Lepton+Jets Final State at DØ Run II,” DØ Note 4874.
- [18] N. Kidonakis and R. Vogt, Phys. Rev. **D68**, 114014 (2003).
- [19] M. Cacciari et al., JHEP **04**, 068 (2004), hep-ph/0303085.